Microvesicle- and exosome-mediated drug delivery enhances the cytotoxicity of Paclitaxel in autologous prostate cancer cells

Heikki Saari [a,1], Elisa Lázaro-Ibáñez [a,1], Tapani Viitala [a], Elina Vuorimaa-Laukkanen [b], Pia Siljander [a,c], Marjo Yliperttula [a,*]

[a] Division of Pharmaceutical Biosciences, Centre for Drug Research, Faculty of Pharmacy, University of Helsinki, P.O. Box 56, Viikinkaari 5E, 00014 Helsinki, Finland
[b] Department of Chemistry and Bioengineering, Tampere University of Technology, P. O. Box 541, Korkeakoulunkatu 8, FI33101 Tampere, Finland
[c] Division of Biochemistry and Biotechnology, Department of Biosciences, University of Helsinki, P.O. Box 56, Viikinkaari 9, 00014 Helsinki, Finland

ABSTRACT

Background: Extracellular vesicles (EVs) are naturally occurring membrane particles that mediate intercellular communication by delivering molecular information between cells. In this study, we investigated the effectiveness of two different populations of EVs (microvesicle- and exosome-enriched) as carriers of Paclitaxel to autologous prostate cancer cells.
Methods: EVs were isolated from LNCaP- and PC-3 prostate cancer cell cultures using differential centrifugation and characterized by electron microscopy, nanoparticle tracking analysis, and Western blot. The uptake of microvesicles and exosomes by the autologous prostate cancer cells was assessed by flow cytometry and confocal microscopy. The EVs were loaded with Paclitaxel and the effectiveness of EV-mediated drug delivery was assessed with viability assays. The distribution of EVs and EV-delivered Paclitaxel in cells was inspected by confocal microscopy.
Results: Our main finding was that the loading of Paclitaxel to autologous prostate cancer cell-derived EVs increased its cytotoxic effect. This capacity was independent of the EV population and the cell line tested. Although the EVs without the drug increased cancer cell viability, the net effect of enhanced cytotoxicity remained. Both EV populations delivered Paclitaxel to the recipient cells through endocytosis, leading to the release of the drug from within the cells. The removal of EV surface proteins did not affect exosomes, while the drug delivery mediated by microvesicles was partially inhibited.
Conclusions: Cancer cell-derived EVs can be used as effective carriers of Paclitaxel to their parental cells, bringing the drug into the cells through an endocytic pathway and increasing its cytotoxicity. However, due to the increased cell viability, the use of cancer cell-derived EVs must be further investigated before any clinical applications can be designed.

1. Introduction

Extracellular vesicles (EVs) such as exosomes (EXOs) and microvesicles (MVs) are lipid membrane-bound vesicles that cells secrete into the extracellular environment. EVs contain a variety of molecules from their cell of origin including different species of RNA and proteins, which retain their bioactive properties when delivered to other cells [1]. EV cargo and their overall composition vary according to the parent cell type, its state of activation and/or stress conditions [2]. Additionally, EVs may target specific cells or tissues for cargo delivery [3]. For these reasons, EVs are thought to play a physiologically significant role in the intercellular communication between cells in healthy and pathological conditions. Cancer cells secrete EVs in order to interact with their environment in ways which promote tumor growth. The effects of cancer cell-derived EVs are diverse and they may also depend on their target cells. EVs have, for example, been reported to promote the formation of a suitable cancerous microenvironment [2] or to reduce the anti-cancer immune response [4]. Cancer cells are also an important target of their own EVs, which may enhance their proliferation [5], or transfer some properties of their own phenotype via vesicles, such as drug resistance by RNA- and protein delivery [6].

The current research suggests that EVs are naturally occurring cargo delivery agents which could also be used as vehicles for drug delivery. What would make them especially suitable for this task is the combination of their innate biocompatibility, their capacity to deliver different types of cargo, and their ability to target specific cells. EVs have already been tried for the delivery of different therapeutic agents in in vitro and in vivo experiments, as reviewed in [7]. Notably, EVs have been shown to be able to cross the blood–brain barrier in mice and to deliver siRNA against the protein BACE1 for treatment of Alzheimer's disease

[8] and curcumin to reduce inflammation in the brain [9]. Additionally, EV-mediated delivery has been examined for proteins such as cytosine deaminase [10] and Let-7 miRNA [11], which were shown to mediate their tumor suppressing properties via EVs. Delivery of EVs loaded with chemotherapeutics is one of the most interesting applications of drug delivery, because a targeted delivery could minimize the side-effects of the drugs while still retaining their anti-tumor effects. This approach has been tested in mice, whereby cancer cells were shown to uptake EVs loaded with different chemotherapeutics, resulting in the killing of cancer cells while also reducing the drugs' unfavorable side effects [12].

In this study, we evaluated the use of EVs from two prostate cancer (PCa) cell lines, PC-3 and LNCaP in cell targeting and in the in vitro delivery of Paclitaxel (PtX), a widely used antimitotic cancer therapeutic. The advantage of using autologous cancer cell-derived EVs is that they are uptaken by cancer cells themselves, as well as by the other cells in the tumor microenvironment. However, since cancer cell-derived EVs have been suggested to promote cancer cell survival and proliferation [5], we firstly assessed whether these EVs were capable of promoting proliferation and secondly, whether this effect could still be overcome by a sufficient concentration of PtX. We also studied the dependency of the EV uptake on the vesicle subtype, along with the dosage and the effect of EV surface proteins on the cytotoxic effect of PtX-loaded EVs (PtX-EVs), as well as on the overall uptake. Our results showed that EVs were continuously uptaken by the PCa cells. The EV-borne PtX was delivered into the cells via an endocytic pathway and released into the cell cytosol causing cell death. Most significantly, the EV-mediated delivery enhanced the cytotoxic effect of the drug. These results suggest that autologous EVs may have potential for effective delivery of chemotherapeutics to cancer cells.

2. Materials and methods

2.1. Cell culture

LNCaP and PC-3 PCa cell lines were obtained from the American Type Culture Collection. Both cell types were grown in T-175 flasks to 80% confluence at 37 °C and 5% of CO_2. LNCaP cells were grown in Roswell Park Memorial Institute 1640 medium (RPMI), and PC-3 cells in Dulbecco modified Eagle medium (DMEM/F12), both supplemented with 10% fetal bovine serum and 1% of penicillin/streptomycin (100 units/mL penicillin and 100 μg/mL streptomycin). All reagents were purchased from Gibco, Life Technologies. The fetal bovine serum was vesicle-depleted by an overnight ultracentrifugation at 110,000 ×g, followed by filtration through a 0.22 μm Steritop filter (Millipore).

2.2. EV isolation using differential centrifugation

EVs were isolated from conditioned medium using differential centrifugation as described by Lazaro-Ibañez et al. [13] and reviewed by others [14,15]. In brief, the conditioned medium was centrifuged at 2500 ×g for 25 min to remove cell debris. The supernatant was then centrifuged at 20,000 ×g for 60 min to obtain the MVs and the final supernatant was ultracentrifuged at 110,000 ×g for 1 h to obtain the EXOs. To more precisely define the EV populations isolated in this study, the centrifugal force used for the isolation of each fraction is stated in the text resulting in 20K MV fraction and 110K EXO fraction. The 20K MV and 110K EXO pellets were resuspended in 100 μL of Dulbecco's phosphate buffered saline (DPBS) (Gibco, Life Technologies). To wash and concentrate the collected EV samples, vesicles were suspended in 1 mL DPBS and pelleted by ultracentrifugation at 170 000 ×g, +4 °C for 3 h using Optima MAX-XP ultracentrifuge with rotor TLA-55 (Beckman Coulter). The resuspended pellets, containing a small volume of the supernatant (30–50 μL), were then stored at −80 °C.

2.3. Transmission electron microscopy (TEM)

The 150 mesh formvar copper grids (*EMS™*) were exposed to the Glow Discharge technique (2 min, 2.4 MA). Then, 4 μL of EV samples were individually added onto the grids and incubated for 2 min at 4 °C. Subsequently, the grids were washed with distilled water, negatively stained with 2% aqueous uranyl acetate (System Biosciences, Mountain View) for 2 min and dried out in darkness for 20 min. The samples were analyzed by TEM (FEI Tecnai 12) at 80 kV and Gatan Orius SC 1000B CCD-camera in the EM-unit, University of Helsinki, Helsinki, Finland. For Cryo-EM imaging of EV samples, carbon grids were first purified with the Gatan Solarus (model 950) plasma cleaning system. Three μL of EV samples were then added onto the grids and frozen with Vitrobot (FEI) in liquid nitrogen. The samples were analyzed by JEOL JEM-3200FSC field emission Cryo-TEM in the Nanomicroscopy center, Aalto University, Espoo, Finland.

2.4. Western blot analysis (WB)

The total protein content of cells and EVs was analyzed in triplicates by the MicroBCA protein assay kit (Thermo scientific) according to manufacturer's recommendations. The samples were diluted in DPBS in ratios of 1:100–1:1000 and incubated at 95 °C for 15 min. Varioskan Flash multireader (v.2.4.3) (Thermo Scientific) with a 562 nm absorbance filter was used to analyze the samples. To remove EV surface proteins, the samples were incubated with 0.25% (w/v) trypsin solution (Invitrogen, Life Technologies) at +37 °C for 30 min. The whole cell lysates and EVs were suspended into RIPA buffer (Thermo Scientific) supplemented with a protease inhibitor mixture (Sigma-Aldrich) according to the manufacturer's recommendations and prepared in 2× Laemmli buffer (Bio-Rad) under non-reducing conditions. Equal amounts of protein from EVs and cells were loaded onto 10–12% Mini-PROTEAN TGX™ gels (Bio-Rad). After electrophoresis (100 V, 30 mA), the proteins were transferred onto Protran nitrocellulose membrane (Whatman International Ltd). The membranes were blocked with 5% (w/v) skim milk powder in Tris-buffered saline Tween 20 (TBS-T) and then incubated for 1 h at room temperature (RT) in 5% milk in TBS-T with the following primary antibodies: mouse monoclonal anti-human CD9 (clone ALB 6) (1:200), anti-CD81 (clone 5A6) (1:200), anti-GAPDH (7B) (Santa Cruz Biotechnology) (1:500), anti α-Tubulin (clone 6A204) (1:2000), anti-CD63 (clone H5C6) (1:200) (BD Pharmingen™), and anti-TSG101 (BD Transduction Laboratories) (1:250). After being washed, the membrane was incubated for 45 min in 2.5% milk in TBS-T at RT with goat anti-mouse IgG-HRP secondary antibody (Santa Cruz Biotechnology). Following another wash, the membranes were incubated for 3 min at RT with Luminata TM Crescendo Western HRP Substrate (Millipore) and visualized with Amersham Hyperfilm™ ECL (GE Healthcare Limited).

2.5. Nanoparticle tracking analysis (NTA)

Purified EV samples were analyzed by NTA using Nanosight model LM14 (Nanosight) equipped with blue (404 nm, 70 mW) laser and SCMOS camera. The samples were diluted in DPBS and three 90 s videos were recorded using camera level 13–14. The data was analyzed using NTA software 2.3 with the detection threshold optimized for each sample and screen gain at 10 to track as many particles as possible with minimal background.

2.6. Zeta potential (ZP)

To assess the effect of trypsin treatment on the surface charge of the EVs, zeta potential was measured by using Zetasizer Nano ZS (Malvern Instruments Ltd). Half of the samples were treated with trypsin as described above, while the rest served as a control for the treatment. Particle concentrations from the column-purified samples were measured

by NTA and diluted into approximately 5×10^8 particle/mL concentration, so that all samples had the same particle concentration.

2.7. Preparation of Paclitaxel-loaded EVs

A 50 mM stock solution of Paclitaxel (PtX; Selleck Chemicals) was prepared by dissolving PtX into DMSO-isobutanol (1:1; Sigma-Aldrich). PtX-loaded EVs were prepared by incubating 1×10^8–5×10^9 EVs/mL in 1 mL of 5 μM PtX-DPBS solution for 1 h at 22 °C. For trypsin-treated PtX-EVs, 0.25% trypsin was added to the samples and incubated at 37 °C for 30 min. Next, the samples were centrifuged at 170 000 ×g for 2 h to pellet the EVs. The supernatant containing unbound PtX and trypsin was removed, and the EV-pellet was washed by suspending it in DPBS and pelleting it again at 170,000 ×g.

2.8. Measurement of EV-bound Paclitaxel by UPLC

Acquity UPLC system (Waters) with a 2.1×50 mm Cortecs C18 + column (particle size 2.7 μm) (Waters) was used to measure the concentration of PtX in the samples. The separation was performed with a flow rate of 0.5 mL/min with a gradient liquid phase consisting of 15 mM phosphate buffer pH 2 (A) and acetonitrile (B). The gradient was formulated according to the following table:

Time (min)	%A	%B
0.00	70.0	30.0
3.00	20.0	80.0
3.01	70.0	30.0
4.00	70.0	30.0

Elution was monitored by UV-absorbance at 229 nm. The retention time of PtX was 1.7 min. To measure the PtX concentration of the PtX-EVs samples, pellets of PtX-EVs were prepared as described above (Section 2.7). The pellets were dissolved in acetonitrile, centrifuged at 10,000 ×g, and 10 μL of the supernatant was injected into the UPLC instrument. Prior to the determination of the PtX concentration from the EV pellet, the acetonitrile extraction method was confirmed by spiking non-loaded EV pellets with 1.8 μM PtX. To study the release of PtX from the PtX-EVs into their surrounding solution, a pellet of PtX-EVs was suspended in DPBS and incubated at 37 °C for 24 h. After that, half of the sample was measured and the other half continued the incubation for another 24 h. The 24/48 h samples were centrifuged at 170,000 ×g for 2 h and the concentration of the leaked PtX was measured from each of the resulting supernatants.

2.9. Viability assays

Five thousand trypsin-detached cells were seeded in a black 96-well plate (CulturPlate, PerkinElmer), leaving five wells empty for background measurements and the outermost wells filled with sterile water. Cells were grown for two days before replacing the growth medium with fresh medium containing either PtX alone, EVs or PtX-EVs. For PtX cell cytotoxicity assays without EVs, different concentrations of PtX were prepared from the stock $1000 \times$ PtX solution into DMSO-isobutanol, which was then added to the culture medium at a ratio of 1:1000. Cell viability was measured after 24, 48, and 72 h by using the AlamarBlue viability assay according to manufacturer's instructions (Life Technologies). Fluorescence intensity was measured using VarioSkan Flash multireader with 560 nm excitation and 590 nm emission filter settings. The viability values were then calculated from the fluorescence intensity values as a percentage of the control cells after removing the mean background values.

2.10. Fluorescent labeling of EVs

EVs were double-labeled with DiD lipophilic dye (Biotium) and OregonGreen-labeled PtX (OG-PtX), (Invitrogen) to study the cellular distribution of PtX-EVs. First, the EVs were incubated for 1 h at RT with 5 μL of DiD per mL of EV suspension in DPBS. The unbound dye was removed by size exclusion chromatography (SEC) and the particle concentration was determined by NTA before labeling with OG-PtX. Next, 5×10^9 vesicles were incubated with 1 μL of OG-PtX (5 μM final concentration) in 1 mL of DPBS for 1 h at RT. For the colocalization studies of EVs and endosomes/lysosomes, the EVs were labeled with DiO lipophilic dye (Biotium) and washed by ultracentrifugation as described previously in Section 2.7 and the cells were labeled with 70 nM LysoTracker® Red (Invitrogen) for 2 h and washed prior to imaging. For the uptake experiments, EVs were labeled with 2 μg/mL of DilC18(5)-DS red dye (Life Technologies) for 20 min at 37 °C protected from light. Then, the EVs were pelleted by ultracentrifugation at 170,000 ×g for 2 h and the pellet was washed as previously described in Section 2.8 before suspending it into 1 mL of cell culture medium.

2.11. Size exclusion chromatography (SEC)

The EVs were purified by size exclusion chromatography as described by Böing et al. [16] to remove unbound dyes and protein fragments after trypsin-treatment for ZP measurements. The presence of EVs in the eluted fractions was confirmed with NTA, with the highest concentrations of vesicles usually found in fractions 8 and 9.

2.12. Uptake experiments

5×10^5 PC-3 cells and 3×10^5 LNCaP cells were seeded in 6-well plates (Corning Costar, Sigma-Aldrich) at 70% confluence. The cells were then washed with DPBS and incubated with cell culture medium containing 10^8–10^9 particles/mL of the 20K MVs- or the 110K EXOs. Following this, the cells were incubated with their autologous EVs for 1, 3, 6, 9, 12, 24, 32, and 48 h. Cells without EVs were used as negative controls. At each time point, the supernatant was removed and the wells were washed two times with DPBS. Cells were detached by trypsin treatment and after several washes fixed with 4% paraformaldehyde in DPBS at 37 °C for 15 min. 10,000 events were analyzed within 6 h by flow cytometry (Gallios, Beckman Coulter) using FL6 channel (638 nm laser). To analyze the internalized and surface-associated EVs, the geometrical mean fluorescence intensity of the cells was determined. Flow-Check™ Pro Fluorospheres (Beckman Coulter) were measured in order to verify fluidics and laser alignment. Data was processed by using FlowJo software 10.0.

2.13. Live cell microscopy

Microscopy studies were performed using a TCS SP5II HCS A (Leica) confocal microscope and a 3I Marianas (3I intelligent Imaging Innovations) wide field microscope with respective $63\times$ water immersion objectives. The PC-3 and LNCaP cells (50,000–100,000 cells) were seeded on a 3 cm culture dish with a poly-D-lysine coated glass coverslip (Mattek) two days prior to the imaging. On the imaging day, the cells were given the labeled EVs, free PtX, PtX-EVs or a combination. The cells, incubated with labeled PtX-EVs, were followed for the first 6 h, recording z-stacks covering the cells' thickness, and then additional images were taken after 24 and 48 h of incubation. Finally, the images were processed with Fiji ImageJ 1.49c.

2.14. Statistical analysis

Statistical analyses were carried out using SPSS 22.0 and SigmaPlot 11.0. The significance of cell viability measurements were tested against the control groups using one-way ANOVA with Tamhane's T2 post hoc

t-test with 95% and 99% confidence intervals. The effect of trypsinization on cell viability and the ZP of EVs were examined using independent sample and paired sample t-tests respectively. The protein amount per particle for the 20 MVs and the 110K EXOs from both cell lines was analyzed using the Mann–Whitney Rank Sum Test.

3. Results

3.1. PCa EV subpopulations differ in terms of protein content and zeta potential

20K MV- and 110K EXO-enriched EV subpopulations were isolated from the conditioned media by using a differential ultracentrifugation with a yield of 10^{11}–10^{12} particles/mL (approximately 250 mL of media in one isolation round). The isolated EV populations were characterized by TEM, NTA, total protein content, and WB analyses (Fig. 1). Based on these results and because at the moment there is no clear consensus in the EV field to distinguish the MV and the EXO subpopulations from each other [14,15], we renamed the subtypes with the speed used for their isolation. The 110K EXOs were often <200 nm in diameter and they showed an artificial cup-shaped morphology when analyzed by TEM (Fig. 1A), while the 20K MVs were a heterogeneous population

mostly >200 nm in diameter (Fig. 1B). On the other hand, the size of both populations overlapped when measured by NTA, which was a result of the heterogeneity of the EV preparations by differential centrifugation (Fig. 1C–D). When the ratio of protein per particle was analyzed from both PCa cell lines, 110K EXOs had significantly more protein than 20K MVs (p-value ≤ 0.003) (Fig. 1E), which were on average 6.88×10^{-9} protein/particle for LNCaP 20K MVs and 2.7×10^{-8} protein/particle for LNCaP 110K EXOs; and 2.98×10^{-8} protein/particle for PC-3 20K MVs and 7.02×10^{-8} protein/particle for PC-3 110K EXOs. Assessing the common EV protein markers CD9, CD81, CD63, and TSG101 by WB showed that they were all enriched in the EVs compared with the cells, regardless of the EV subpopulation. Also, α-tubulin and GAPDH were found to be present in the PCa EVs (Fig. 1F).

Trypsin treatment of EVs did not damage the EV structure (Fig. 2A–B), but almost completely removed the surface proteins of the 20K MVs and 110K EXOs, as shown for the transmembrane proteins CD9 and CD63 (Fig. 2C). In addition, the ZP of EVs was mildly but not statistically significantly affected by trypsin treatment. EVs from both cell lines had similar ZP values (Fig. 2D). The mean ZP was approximately −11.90 mV for the 110K EXOs and −11.22 mV for the 20K MVs. Cleavage of the surface proteins affected the subpopulations differently: the ZP of
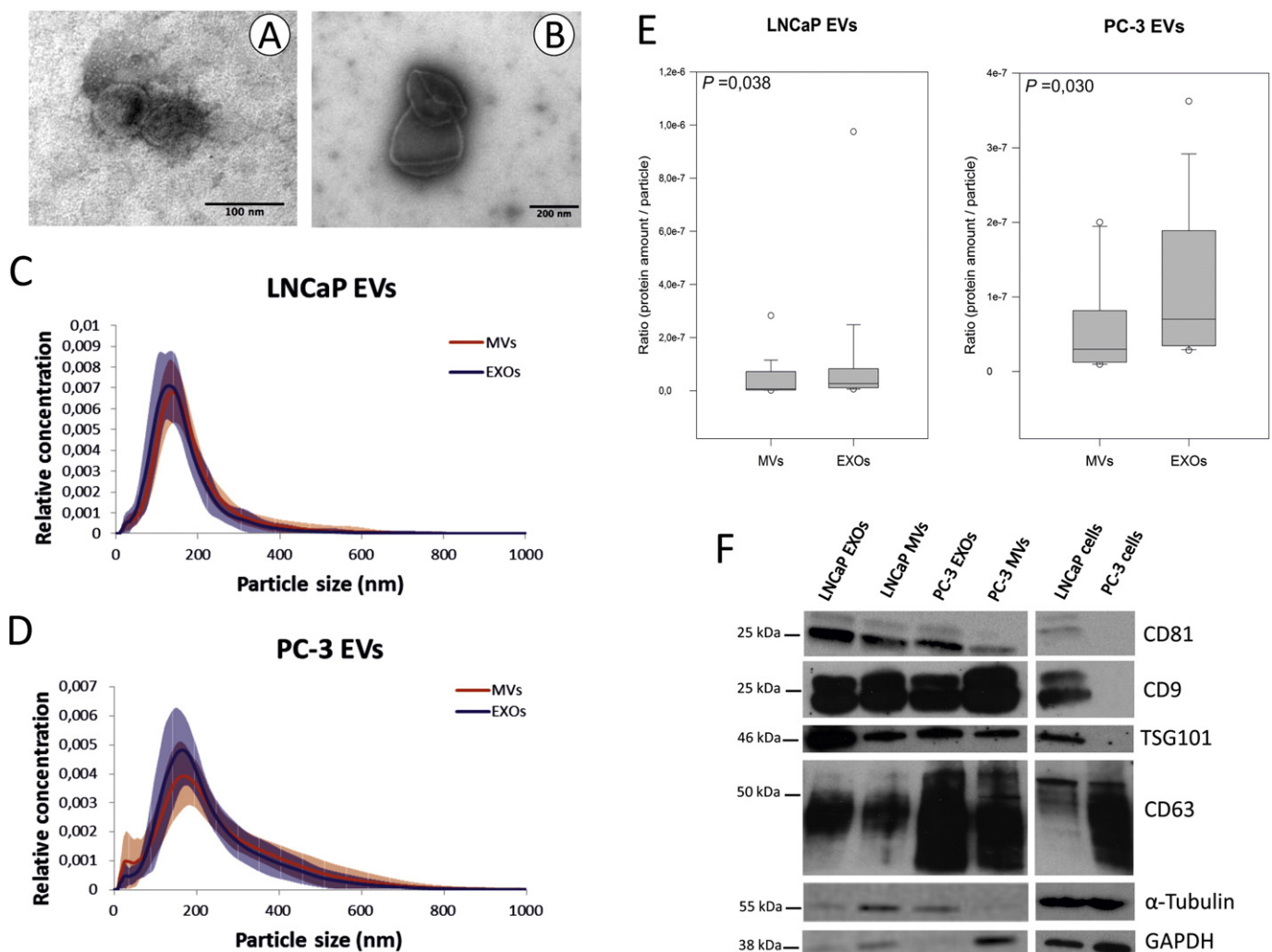
Fig. 1. Characterization of PCa cell-derived EVs. A–B) Representative transmission electron microscopy images of negatively stained PC-3 110K exosomes (EXOs, A) and 20K microvesicles (MVs, B). The scale bar is included in each figure. C–D) NTA measurements showing the size distribution of (C) LNCaP MVs (n = 21) and EXOs (n = 21) and (D) PC-3 MVs (n = 24) and EXOs (n = 23). The continuous lines represent the mean value of the samples. Shaded areas show the ±SD. E) Box plots showing the ratio of protein per particle for LNCaP MVs (n = 24), LNCaP EXOs (n = 22), PC-3 MVs (n = 16), and PC-3 EXOs (n = 15). Error bars represent ±SE. p-values were determined by the Mann–Whitney Rank Sum Test. F) Western blots of PCa cell lysates and PCa-derived MVs and EXOs showing the expression of CD81, CD9, TSG101, CD63, α-Tubulin and GAPDH. 50 μg of protein was loaded per lane. The panels are a representative of n ≥ 3 independent protein preparations showing the same trend.
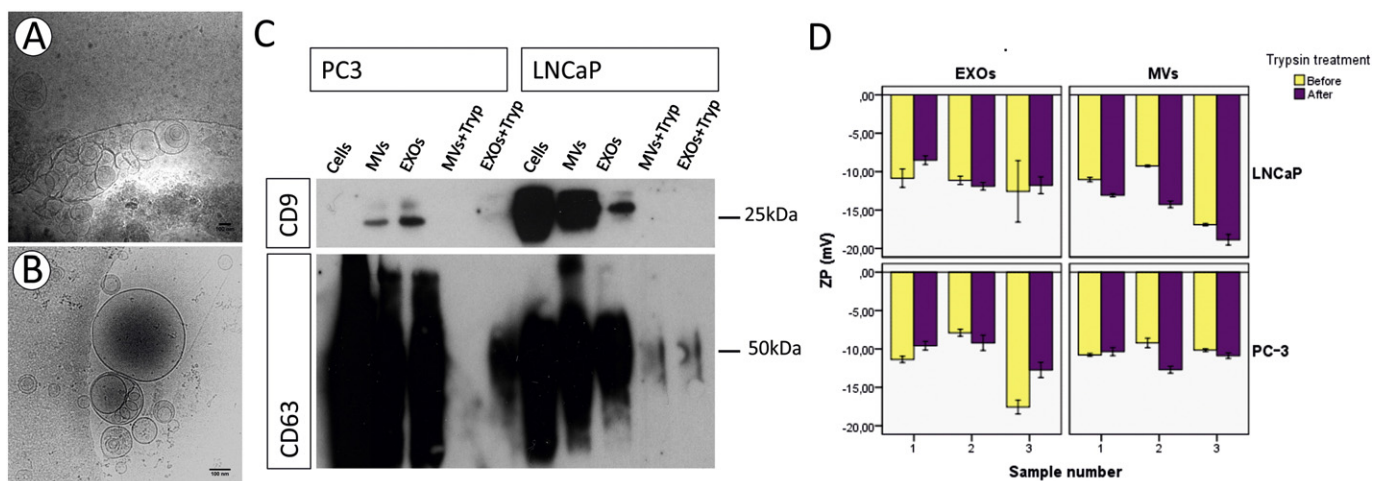
Fig. 2. Effect of trypsin treatment in EVs. A–B) Visualization of trypsinized (A) vs. non-trypsinized (B) LNCaP-derived 20K MVs by Cryo-EM. Spherical vesicles with a lipid bilayer can be observed, but no broken vesicles. Scale bars: 100 nm. C) A representative figure of the Western blot of trypsinized and non-trypsinized 20K microvesicles (MVs) and 110K exosomes (EXOs). The EV markers CD9 and CD63 were assessed by Western blotting before and after trypsin treatment. 50 μg of protein was loaded per lane. This panel is representative of three independent protein preparations showing the same trend. Very low amounts of CD9 and CD63 proteins remained after trypsin treatment. D) Zeta potential measurements of trypsinized and non-trypsinized EVs. N = 3; error bars represent ±SE. p-values were determined by a paired t-test.

most of the 110K EXO samples became on average 8% less negative and the ZP of most the 20K MVs became on average 21% more negative. The average ZP-values after trypsin treatment in all the samples changed to −10.51 mV for the 110K EXOs ($p = 0.221$) and −13.35 mV for the 20K MVs ($p = 0.043$).

3.2. PCa cells efficiently uptake autologous EVs

To study their cellular uptake and the intracellular trafficking of EVs, LNCaP and PC-3 cells were incubated with their own DilC18(5)-DS-labeled vesicles for different time periods (1–24 h). EVs from both PCa cell lines were actively and continuously bound and internalized (Fig. 3A) when analyzed by flow cytometry. The internalization increased as a function of time with no differences in the efficiency of LNCaP and PC-3 uptake. At the early time points (1–3 h), there was a lag in the fluorescence intensity which was followed by an increase in the uptake after 6 h continuing further to 24 h (Fig. 3A) and 48 h (Fig. 3B), the end of the follow-up period. When the uptake of these EVs was compared with the trypsin-treated vesicles (Fig. 3B), no significant differences were observed between the trypsin-treated and the

non-treated 110K EXOs, indicating that the uptake was not determined by the surface proteins. However, the uptake of the 20K MVs was notably decreased as a result of the treatment, suggesting that surface proteins were at least partially involved in the uptake of the 20K MVs.

3.3. PCa-derived EVs increase cell viability

To study the capacity of PCa-derived EVs to influence cancer cell viability, PC-3 and LNCaP cells were incubated with different EV subtypes and the change in their viability was measured against an EV-free control group after 24 and 48 h(Fig. 4). Both the 20K MVs and the 110K EXOs increased the cell viability of their respective cell lines. In PC-3 cells, there was a clear difference between the two populations of EVs with the 110K EXOs(Fig. 4D) having a stronger viability increasing effect than the 20K MVs(Fig. 4C), which was most apparent after 48 h of incubation. In LNCaP cells, the 110K EXOs (Fig. 4B) seemed to have a slightly stronger effect than the 20K MVs (Fig. 4A) at both time points. In general, the effect of EVs was found to be dose-dependent, although in the case of PC-3 20K MVs, a similar effect was observed with all doses examined.
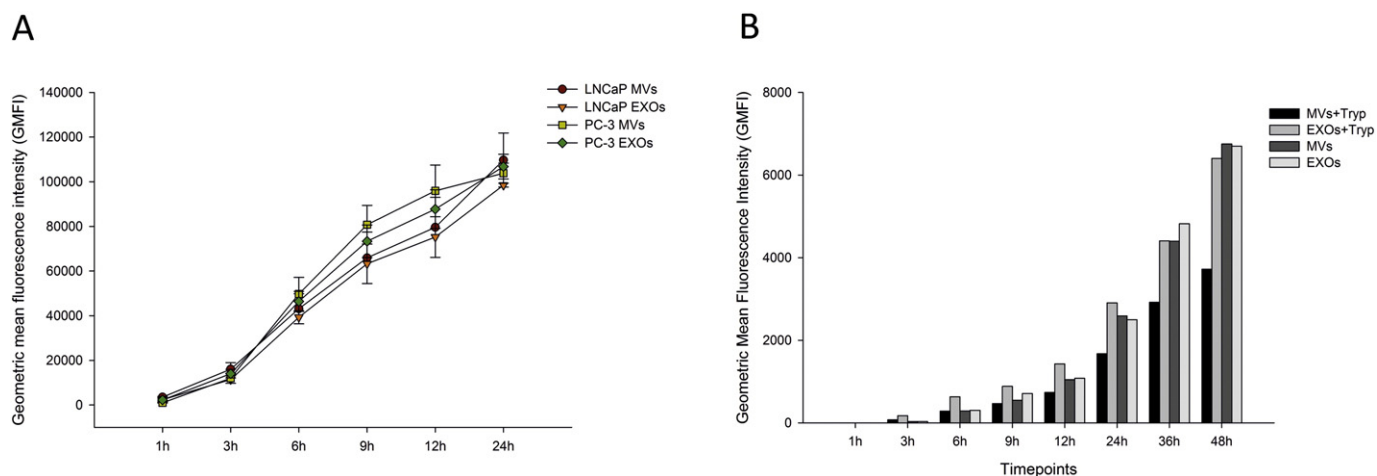
Fig. 3. Uptake of EVs by PCa cells as function of time. A) LNCaP and PC-3 cells were incubated with their own DilC18 (5)-DS labeled 20K microvesicles (MVs) and 110K exosomes (EXOs) for various time periods up to 24 h. EV uptake was measured by determining the geometric mean fluorescence intensity of the cells. The mean ± SE of three independent experiments are shown. B) Comparison of the uptake of the trypsinized vs. non-trypsinized PC-3 cell-derived EVs. The geometric mean fluorescence intensities of PC-3 cells were determined after their incubation with the trypsin treated and the non-treated MVs and EXOs at several time points up to 48 h.
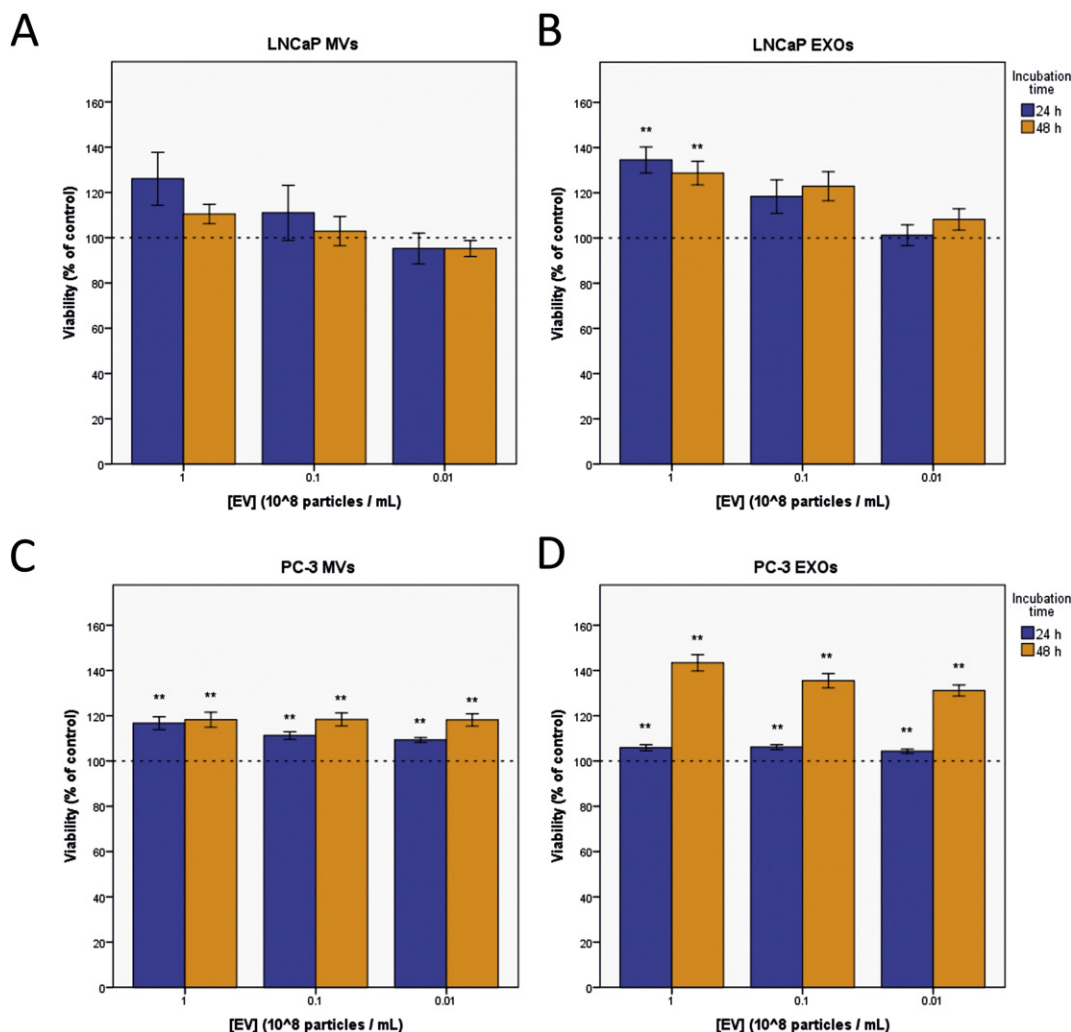
Fig. 4. PCa-derived EVs increase cell viability. The uptake of 20K microvesicles (MVs) and 110K exosomes (EXOs) by the PCa cells increased the cell viability independently of the EV population or the cell line. A) LNCaP cells incubated with LNCaP derived MVs (n = 4) and B) EXOs (n = 4), C) PC-3 cells incubated with PC-3 derived MVs (n = 6) and D) EXOs (n = 6). Error bars represent ±SE. Significant differences against the untreated control group observed with a *95% or **99% level of confidence were determined with a t-test. Dashed line indicates the viability of the control PCa cells grown in the absence of EVs (100%).

3.4. Cytotoxicity of PtX can be enhanced by EV-mediated delivery

The cytotoxic effect of the PtX-EVs on autologous PCa cells was compared to the free drug by viability assays. Cell viability curves were established as a function of PtX-EV dose for both PC-3 and LNCaP cells (Fig. 5 and S2). 5 μM PtX served as a point of comparison for the cell viability assays of PtX-EVs, since higher drug concentrations were found to precipitate in the solution. First, PtX-EVs were prepared with a high concentration of EVs (5×10^9 particles/mL) in the 5 μM PtX loading solution (ratio of 1 nmol of PtX/10^9 EVs). After removal of the unbound drug, a dilution series was utilized with both of the cell lines to establish the dose-dependency of the PtX-EVs. According to the UPLC measurements of the EV-bound PtX, approximately 9.2% (SD ± 4.5%) of the drug was bound to the EVs on average as a result of the loading regardless of the EV-concentration (Table 1). The final PtX concentration in the PtX-EV preparations was 0.46 μM on average (SD ± 0.22 μM). Confocal microscopy images of DiD-labeled EVs and OG-labeled PtX showed colocalization of the drug with the EVs, while no detectable staining of the cells' microtubules by free OG-PtX was observed after one hour of incubation (Fig. S1). Additionally, UPLC measurements of the amount of PtX released from the PtX-EVs incubated in 37 °C for 24 and 48 h after loading revealed that no detectable amounts of PtX were leaking into their surrounding medium during this time ($n_{20K\ MVs} = 3$, $n_{20K\ EXOs} = 3$).

The dose-dependent cytotoxic effect of free PtX was clearer on PC-3 cells than LNCaP cells, which responded similarly to all different concentrations of the drug (Figs. 5A and S2.A). The maximum decrease in PC-3 cell viability was about 40% after 24 h (max mean difference 41.3, SE ± 3.16, $p = 3.6 \times 10^{-10}$) and 60% after 48 h (max mean difference 63.5, SE ± 1.54, $p < 10^{-15}$) from concentrations of 50 nM and above, while the cytotoxic effect of PtX at 10 nM and below was significantly smaller (16% at 24 h and 27% decrease 48 h, $p = 4.63 \times 10^{-4}$ and 1.45×10^{-7}, respectively). In LNCaP cells, viability consistently decreased to approximately 80% and 60% after 24 and 48 h respectively, regardless of the dose (Fig. S2.A). Incubating the cells directly with free PtX and unloaded EVs resulted in the reduction of the cytotoxic effect at the 24 hour timepoint compared to the cytotoxicity of PtX-EVs, but the effect was similar to the EV-free 5 μM PtX control at 48 h (Fig. S2.B). For both cell lines and EV subtypes, a saturation point was reached approximately at 10^9 PtX-EVs/mL (Figs. 5B–C and S2.C–D). At this and higher concentrations, maximal cytotoxic effect of PtX-EVs was observed, while at lower concentrations PtX-EVs had a lesser or even a viability enhancing effect. At 48 h, the maximal cytotoxic effect of PtX-EVs was lower than with the 5 μM free PtX except for the PC-3 PtX-20K MVs, which exceeded the cytotoxicity of the free PtX. Finally, the viability enhancing effect of low concentrations of the PtX-110K EXOs was similar to what was observed with the unloaded EVs at corresponding concentrations.
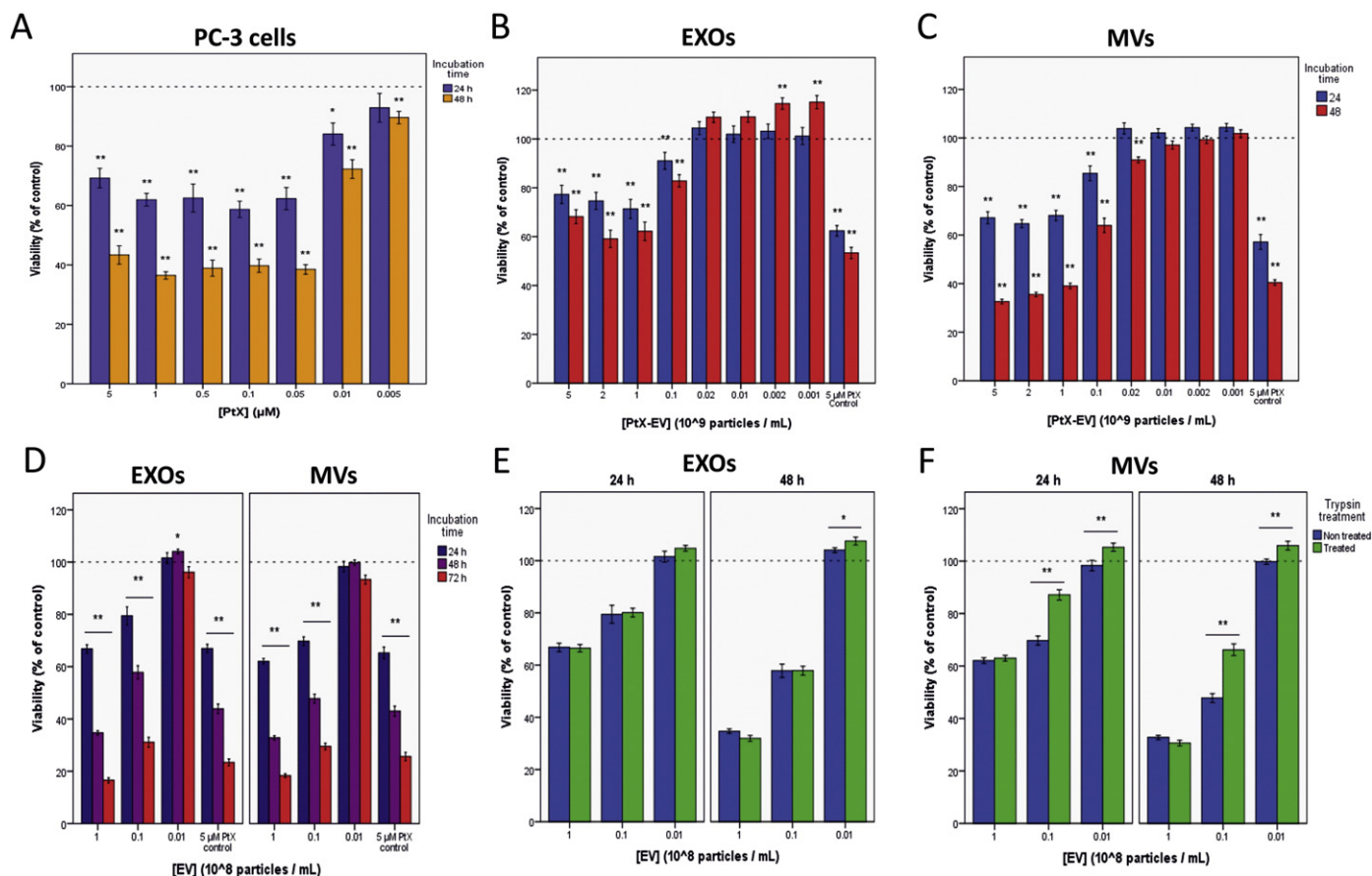
Fig. 5. Paclitaxel (PtX) delivered to the PCa cells by EVs enhances its cytotoxicity compared to free PtX. Cell viability experiment were conducted to evaluate the cytotoxic effect of free and EV-loaded PtX. PtX maintained its cytotoxic effect at 24 and 48 h when delivered to the cells by EVs. The cytotoxic effect on cell viability was dependent on the EV concentration and the amount of PtX per vesicle. A) Representative graph of three independent experiments with five replicates of PC-3 cells incubated with different concentrations of PtX. Representative graphs of three independent cytotoxicity experiments with five replicates of PC-3, B) 110K exosomes (EXOs) and C) 20K microvesicles (MVs) loaded with 1 nmol of PtX per 10^9 vesicles. D) Representative graphs from five independent experiments with five replicates of the cytotoxic effect of PC-3 EVs loaded with 5 nmol of PtX per 10^8 vesicles at 24, 48, and 72 h. E–F) Comparison of the cytotoxic effect of the trypsinized and the non-trypsinized PtX-MVs (E) and -EXOs (F) loaded with 5 nmol of PtX per 10^8 vesicles at 24 and 48 h. The graphs are representative of 6 independent experiments with 5 replicates. In all cases, error bars ± SE. Significant differences determined with t-test with *95% or **99% level of confidence. Dashed line indicates the 100% viability of control PCa cells in the absence of EVs and PtX.

Next, PtX-EVs were prepared with an EV concentration below the apparent saturation point to examine whether a non-saturating number of EVs loaded with more drug per vesicle would have had a stronger cytotoxic effect. 10^8 EVs/mL were loaded in 5 μM PtX, corresponding to a drug per vesicle ratio 50 times higher than used in the previous experiment. The cytotoxic effect of these PtX-EVs was stronger than that of those prepared with less PtX per vesicle, and it also exceeded the effect of the PtX-control at 48 h with both EV subpopulations (Fig. 5C). Increasing the amount of free PtX beyond 5 μM in the control groups did not increase its cytotoxic effect, so the effect of 5 μM PtX was considered as the maximal cytotoxic effect of free PtX. It was also confirmed that the enhanced cytotoxicity persisted at 72 h of incubation

(Fig. 5D). Further, cytotoxicity also persisted regardless of changing the medium after 48 h. Differences at 48 and 72 h between the cells treated with 5 μM free PtX and the highest concentrations of 110K EXOs/20K MVs were found to be significant with a confidence interval of 99%.

To study the significance of the EV surface proteins in the cytotoxicity of PtX-EVs, the same PtX-EVs were treated with trypsin and compared against non-treated EVs. The trypsin-treated PtX-110K EXOs had an almost identical cytotoxic effect compared to the non-treated PtX-EVs (Fig. 5E). A statistically significant decrease in the cytotoxicity of the trypsin-treated PtX-EVs was apparent only at the lowest concentrations of the PC-3 PtX-20K MVs at 24 and 48 h (Fig. 5F) and at the

Table 1
The amount of PtX per EV after loading. Two different concentrations of the 110K EXOs and the 20K MVs were loaded in 5 μM PtX and the amount of PtX in the PtX-EV pellet was measured with UPLC as described in the Materials and methods.

110K EXOs				20K MVs			
[EV] ($\times 10^8$/mL)	Sample	PtX/EV (pmol/10^8)	EV-bound portion of PtX (%)	[EV] ($\times 10^8$/mL)	Sample	PtX/EV (pmol/10^8)	EV-bound portion of PtX (%)
50	1	2.83	5.66	50	1	6.30	12.60
	2	3.48	6.96		2	3.29	6.57
					3	10.52	21.05
1	1	179.55	7.18	1	1	138.00	5.52
	2	250.65	10.03		2	238.95	9.56
					3	168.15	6.73

lowest concentration of the PtX-110K EXOs at 48 h (Fig. 5E). (*p*-values 1.03×10^{-8} and 1.24×10^{-8} for 10^7 PtX-20K MVs/mL and 0.0079 and 0.0024 for 10^6 PtX-20K MVs/mL at 24 and 48 h and 0.049 for 10^6 PtX-110K EXOs/mL at 48 h).

3.5. EVs deliver PtX through an endocytic pathway releasing the drug within the cells

To investigate the internalization route of the EVs, we investigated their localization by staining the cells with LysoTracker® Red, a fluorescent marker for labeling acidic organelles such as endosomes and lysosomes (Fig. 6). First, the DiO-labeled EVs were incubated with PC-3 (Fig. 6A) and LNCaP (Fig. 6B) cells for 24 h and the cells were examined by fluorescence microscopy after the addition of LysoTracker® Red. An intracellular fluorescent pattern of green labeled EVs was found to colocalize with the cell endosomal or lysosomal compartments (red), while EVs that had not yet been internalized were found on the plasma membrane. These data demonstrate that the internalized EVs and therefore also the PtX carried by them were delivered into the cells via the endocytic pathway.

Next, LNCaP and PC-3 cells were treated with OG-PtX-loaded DiD-EVs and DiD-EVs with free OG-PtX. When PCa cells were given free PtX from the medium, it spread into the cells binding to the microtubules (Fig. 7C–D). PtX from the medium caused the cells to eventually lose their elongated, branched shape and become spherical before they started dissociating and dying (Fig. 7D). When PtX was delivered into the cells by EVs, PtX was transported into the cells via the endocytic pathway regardless of the EV-subtype used as the vehicle, and then liberated within the cytosol (Fig. 7A–B). In the endosomal network the EV-delivered PtX appeared to eventually separate from the EV-label. After dissociating from the EVs, the PtX spread into the cells. The liberated PtX then stained the microtubules similarly to the staining by the free PtX from the culture medium, albeit more weakly (Fig. 7C–D). Cells were also incubated with free PtX and EVs that were not loaded with the drug. Even though the EVs were not loaded with PtX when they were given to the cells, the OG-PtX was also found in the endosomes, which suggested that the PtX could partially bind to the EVs in the medium. At 24 h, the cells that were still alive with PtX-EVs had taken up notable amounts of EVs and only small or undetectable amounts of PtX-label, which suggested that they had not received sufficient amounts of PtX via EVs to kill them (Fig. 7B).

4. Discussion

The main finding of the present study is that EVs can enhance the cytotoxic effect of PtX when autologous EVs were used to deliver the drug to PCa cells in vitro. Although PtX has previously been shown to be deliverable by EVs [12,17], including autologous cancer cell derived EVs [18], so far, there have not been previous comparisons of the two main populations of EVs as drug carriers with the exception of the study by Zhuang et al. [9], showing that $10,000 \times g$-isolated MVs were less effectively accumulated in the mouse brain than EXOs. Given the heterogeneity of the vesicle populations isolated by the current gold standard differential centrifugation, it is not yet clear which vesicle type will be the best to further optimize for carrying certain amounts of therapeutic cargo. In our study, although the cytotoxicity enhancing effect of PtX by EVs was moderate, it was statistically significant. Both EV populations, the 20K MVs and the 110K EXOs, were capable of enhancing the cytotoxic effect of the drug at high PtX concentrations. However, when a high concentration of EVs was loaded with a relatively low amount of PtX per vesicle, the 20K MVs seemed to be more effective drug carriers than the 110K EXOs. Overall, our study suggests that regardless of their differences, both types of EVs could be useful as biomimetic targeted drug carriers in cancer therapy.

To address the role of EV surface proteins in drug delivery, we assessed the effect of trypsinization on the cellular uptake of EVs and on the cytotoxicity of PtX-EVs. We found that although there were differences, for instance, in the protein content and zeta potential of 20K MVs and 110K EXOs, their cellular uptake and efficiencies as drug carriers were quite similar. The trypsin treatment disrupted surface proteins like CD9 and CD63 present in LNCaP- and PC-3 cell-derived vesicles, but did not significantly affect the uptake of 110K EXOs by their parental cells (Fig. 3B), and their overall efficiency as drug carriers remained quite similar (Fig. 5E). We did observe, however, that the 20K MVs were more sensitive to trypsin treatment in terms of PtX-20K MV cytotoxicity (Fig. 5F), which might be explained by their reduced uptake after the treatment (Fig. 3B). These results suggest that EV-associated protein markers may not be the key players in the vesicle internalization as has been previously reported [19]. The effect of trypsin treatment on
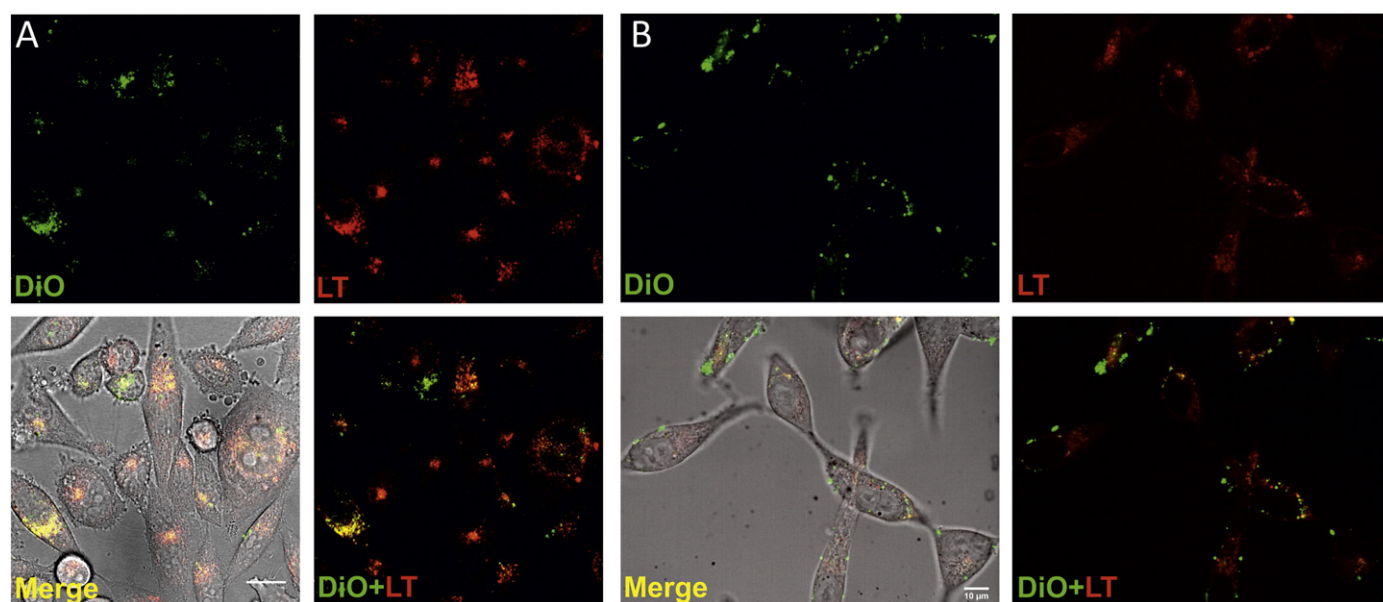
Fig. 6. EVs colocalize with the late endosome/lysosomes. Separated and merged channels of confocal microscopy images are shown. EVs were labeled with DiO green and added to the cultures of A) PC-3 cells and B) LNCaP cells respectively. After 24 h, the cells were stained with LysoTracker® Red, washed with medium and analyzed by confocal microscopy. Scale bar, 20 and 10 μm respectively.
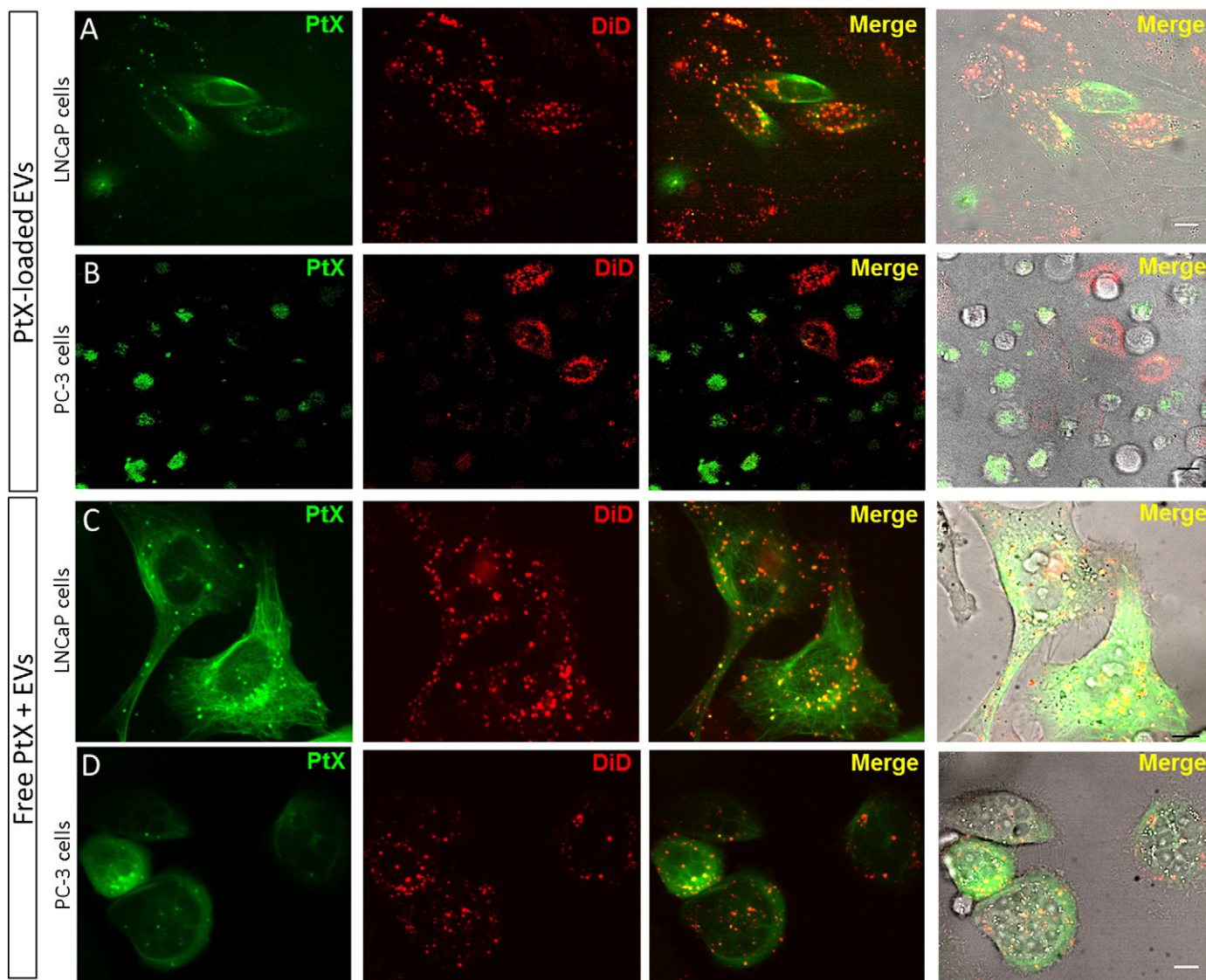
Fig. 7. Intracellular distribution of free Paclitaxel (PtX), PtX-loaded EVs and combined free PtX and EVs in LNCaP and PC-3 cells at 24 h of incubation. Separate and merged channels of confocal microscopy images are shown. A) LNCaP cells incubated with PtX-loaded EVs. Scale bar of 10 μm. B) PC-3 cells incubated with PtX-loaded EVs. Scale bar of 20 μm. C) LNCaP and D) PC-3 cells incubated with free OG-PtX and unloaded EVs. Scale bars of 10 μm. In all cases, representative images are shown from experiments with 5–12 different imaging positions. All images were taken after 24 h incubation. Before imaging, several washes were performed to remove the unbound vesicles and free PtX. The z-stacks were about 20 images in total and the representative images were taken at the focal plane of the bright field channel.

the ZP of EVs was inconclusive, although there was an apparent trend, reducing the negative charge of the 110K EXOs and increasing the ZP of the 20K MVs. The overall surface charge of EVs is likely to be dominated by the charged lipids of the membrane, but the surface proteins might also provide a shielding effect masking the lipids partially. Thus, their removal might have an unpredictable effect. Besides membrane proteins, the relevance of other EV membrane components for the vesicle uptake, such as the lipid signatures [19] has been suggested, while some pathways such as micropinocytosis might not require any specific interaction at all between the cell and EVs [20]. In any case, more research should be done to investigate the critical factors and the molecular components determining EV uptake and targeting.

One of the challenges associated with EVs as future drug delivery vehicles is their capacity to load drugs efficiently. Different methods for loading therapeutic cargo into EVs (electroporation, transfection, cell activation, and incubation) have been assessed, reviewed in [7]. In this study, we incubated EVs with PtX to load them with the drug by passive diffusion, taking advantage of the high lipophilicity of PtX, with a log P value of 3.96 and very poor aqueous solubility of less than 0.01 mg/mL

[21]. This loading strategy yielded an average loading efficiency of 9.2% in all our samples. The efficiency of loading has been shown to depend on the hydrophobic nature of the drug, as no major differences were found between passive diffusion and electroporation of hydrophobic porphyrins into EVs [22]. Also, the small size of the molecules, e.g. doxorubicin [23,24], PtX [18] or curcumin [9,25], loaded by this technique may facilitate their passage across the vesicle membrane [7]. These same properties, however, may allow the molecules to move out of the EVs. In a study by Smyth et al. [24], it was reported that after 24 h approximately 70% of doxorubicin incorporated into EVs by passive diffusion had leaked out. When measured by UPLC, the leakage of PtX from the EVs in our study was minimal, which could be dependent on the poorer water solubility of PtX. Another EV loading method that has been successfully exploited is the feeding of desired compounds, including PtX, to cultured cells [12,17] or genetically engineering them to produce RNA or proteins [3,11], which then become partially incorporated into the secreted EVs. While this approach is also nondestructive, the loading is difficult to control and it might affect the targeting and other biological properties of the produced EVs.

To our knowledge, this is also the first study to assess the PtX- and EV -dose dependency of the cytotoxicity. We initially identified a possible saturation point of PtX-EVs by testing concentrations of PtX-EVs over a wide scale, and an EV concentration below the saturation point to optimize EV-mediated PtX uptake. The identified saturation point was consistently 10^9 PtX-EVs/mL, at which point the maximal cytotoxic effect was reached. Subsequently, using a lower concentration of EVs increased the cytotoxic effect of PtX compared to the free drug. On the other hand, EV concentrations above the saturation point generally had a less cytotoxic effect compared to the free PtX. These results suggested that a combination of a high amount of drug per vesicle and a number of EVs below the saturation point generate the highest cytotoxic effect. The UPLC measurements of PtX carried by EVs suggested that a similar amount of the drug could bind to 20K MVs and the 110K EXOs during the PtX-loading in the high- and low EV-concentration containing conditions. However, to produce the enhanced cytotoxic effect on the autologous PCa cells, the 110K EXOs required a higher PtX/EXO ratio, whereas the 20K MVs had a similar cytotoxicity enhancing effect regardless of the PtX/MV ratio. A possible explanation for this difference could be that the 110K EXOs were more effective at increasing the viability of cancer cells and thereby partially counteract the effect of PtX. However, since the uptake of unloaded EVs by cancer cells continued over 48 h, it could be presumed that eventually all of the drug would be taken up by the cells via the EVs, which should then lead to the same result as with less EVs. It is possible that PtX might eventually inhibit the uptake of additional PtX-EVs by stabilizing the microtubules of the recipient cells, which would hinder the endocytic pathway [26].

The enhanced cytotoxic effect of PtX-EVs could not be explained by the presence of free PtX. Firstly, no detectable leaking of free PtX from the loaded EVs was observed, although small residues may have been present in our PtX-EV preparations regardless of their washing. Secondly, incubating cells with 5 μM free PtX and EVs without PtX-loading (Fig. S2.A) only resulted in a lag of the PtX-induced cytotoxicity without enhancing it. Currently, we have no explanation why EVs can enhance the cytotoxic effect of PtX. The answer could be that EVs are able to carry more drug into the cells than what the cells gather from the surrounding medium as has been shown earlier [12]. Another possible explanation for the enhanced cytotoxicity could be that the EVs deliver the drug into an optimal subcellular location. Besides β-tubulin, PtX has another binding target, Bcl-2, an apoptosis regulator [27], which is a membrane protein found in the membranes of the endoplasmic reticulum, nucleus and mitochondria. By binding to Bcl-2, PtX has been shown to promote apoptosis [27], and by bringing the drug to the proximity of Bcl-2, EVs might enhance its cytotoxic effect. Consistent with our microscopy studies, it has previously been shown that EVs are delivered into the cell primarily by the endocytic pathway [26]. Here, we also showed that PtX was carried into the cells by EVs through endocytosis and that PtX dissociated from the EVs inside the cells, which lead to an uneven distribution of the drug from within the cell cytosol.

Although the EVs as delivery vehicles could enhance the cytotoxic effect of PtX, there may be risks involved with their use for clinical purposes. As shown here, and consistent with the findings of others [5], the cancer cell-derived unloaded EVs increased the viability of cancer cells. The effect was more notable in the case of 110K EXOs, which seemed to enhance cell viability more than 20K MVs, and a larger dose of the drug was required to counteract this viability increasing effect. In contrast, EVs from non-cancerous cells may be capable of suppressing tumor proliferation [28], which would make them an attractive alternative to cancer cell-derived EVs [17,18]. On the other hand, several functional studies have shown that EVs derived from tumor cells may adopt the same repertoire of surface receptors and extracellular matrix-binding proteins as their parental cell of origin [3,29], which is different from those of non-malignant cells. This could be used as an advantage to increase the specificity of targeting and uptake to tumor tissues. However, there could still be collateral damage in the form of macrophages, which can also devour EVs hindering delivery to cancer cells and dying as a result [12,30]. Finally, another important aspect for using EVs as drug carriers is that the EV-mediated cancer cell targeting could help to reduce the side effects of the drugs [12]. Therefore further studies, especially in vivo models, need to be developed for the improved targeting and pharmacokinetics of cancer-derived EVs as drug delivery vehicles.

5. Conclusions

As a proof of concept, we have demonstrated in this study that autologous cancer cell-derived EVs could be useful drug delivery vehicles in the treatment of cancer, since the EV-mediated delivery enhanced the cytotoxic effect of the used drug, PtX. A relatively small concentration of EVs loaded with a higher amount of PtX generated the best cytotoxic effect in autologous cells. Although the uptake of EVs was found to be continuous, a saturation point in the cytotoxicity of PtX-EVs could be identified. Despite the slight differences between the two EV populations isolated by the standard ultracentrifugation technique, the 20K MVs and the 110K EXOs were almost equally effective, capable of promoting the cytotoxicity of PtX even after the removal of their surface proteins. EVs delivered PtX into the cells via the endocytic pathway and the drug was subsequently released from within the cell, in contrast to being absorbed from the cell surroundings, as the free PtX. Although these results provide support for the use of cancer cell EVs derived from patients own cells in drug delivery, the viability enhancing effects and tailored targeting of these EVs must be well addressed before clinical applications will become possible.

Supplementary data to this article can be found online at http://dx.doi.org/10.1016/j.jconrel.2015.09.031.

References

[1] J. Skog, T. Würdinger, S. van Rijn, D.H. Meijer, L. Gainche, W.T. Curry, B.S. Carter, A.M. Krichevsky, X.O. Breakefield, Glioblastoma microvesicles transport RNA and proteins that promote tumour growth and provide diagnostic biomarkers, Nat. Cell Biol. 10 (2008) 1470–1476.

[2] M. Wysoczynski, M.Z. Ratajczak, Lung cancer secreted microvesicles: underappreciated modulators of microenvironment in expanding tumors, Int. J. Cancer 125 (2009) 1595–1603.

[3] S. Rana, S. Yue, D. Stadel, M. Zoeller, Toward tailored exosomes: the exosomal tetraspanin web contributes to target cell selection, Int. J. Biochem. Cell Biol. 44 (2012) 1574–1584.

[4] M. Szajnik, M. Czystowska, M.J. Szczepanski, M. Mandapathil, T.L. Whiteside, Tumor-derived microvesicles induce, expand and up-regulate biological activities of human regulatory T cells (Treg), PLoS One 5 (2010) e11469.

[5] J. Qu, X. Qu, M. Zhao, Y. Teng, Y. Zhang, K. Hou, Y. Jiang, X. Yang, Y. Liu, Gastric cancer exosomes promote tumour cell proliferation through PI3K/Akt and MAPK/ERK activation, Dig. Liver Dis. 41 (2009) 875–880.

[6] C. Corcoran, S. Rani, K. O'Brien, A. O'Neill, M. Prencipe, R. Sheikh, G. Webb, R. McDermott, W. Watson, J. Crown, L. O'Driscoll, Docetaxel-resistance in prostate cancer: evaluating associated phenotypic changes and potential for resistance transfer via exosomes, PLoS One 7 (2012) e50999.

[7] K.B. Johnsen, J.M. Gudbergsson, M.N. Skov, L. Pilgaard, T. Moos, M. Duroux, A comprehensive overview of exosomes as drug delivery vehicles—endogenous nanocarriers for targeted cancer therapy, Biochim. Biophys. Acta Rev. Cancer 1846 (2014) 75–87.

[8] L. Alvarez-Erviti, Y. Seow, H. Yin, C. Betts, S. Lakhal, M.J. Wood, Delivery of siRNA to the mouse brain by systemic injection of targeted exosomes, Nat. Biotechnol. 29 (2011) 341–345.

[9] X. Zhuang, X. Xiang, W. Grizzle, D. Sun, S. Zhang, R.C. Axtell, S. Ju, J. Mu, L. Zhang, L. Steinman, Treatment of brain inflammatory diseases by delivering exosome encapsulated anti-inflammatory drugs from the nasal region to the brain, Mol. Ther. 19 (2011) 1769–1779.

[10] A. Mizrak, M.F. Bolukbasi, G.B. Ozdener, G.J. Brenner, S. Madlener, E.P. Erkan, T. Stroebel, X.O. Breakefield, O. Saydam, Genetically engineered microvesicles carrying suicide mRNA/protein inhibit schwannoma tumor growth, Mol. Ther. 21 (2013) 101–108.

[11] S. Ohno, M. Takanashi, K. Sudo, S. Ueda, A. Ishikawa, N. Matsuyama, K. Fujita, T. Mizutani, T. Ohgi, T. Ochiya, Systemically injected exosomes targeted to EGFR deliver antitumor microRNA to breast cancer cells, Mol. Ther. (2012).

[12] K. Tang, Y. Zhang, H. Zhang, P. Xu, J. Liu, J. Ma, M. Lv, D. Li, F. Katirai, G. Shen, Delivery of chemotherapeutic drugs in tumour cell-derived microparticles, Nat. Commun. 3 (2012) 1282.

[13] E. Lázaro-Ibáñez, A. Sanz-Garcia, T. Visakorpi, C. Escobedo-Lucea, P. Siljander, Á. Ayuso-Sacido, M. Yliperttula, Different gDNA content in the subpopulations of prostate cancer extracellular vesicles: apoptotic bodies, microvesicles, and exosomes, Prostate 74 (2014) 1379–1390.

[14] B. Gyoergy, T.G. Szabo, M. Pasztoi, Z. Pal, P. Misjak, B. Aradi, V. Laszlo, E. Pallinger, E. Pap, A. Kittel, G. Nagy, A. Falus, E.I. Buzas, Membrane vesicles, current state-of-the-art: emerging role of extracellular vesicles, Cell. Mol. Life Sci. 68 (2011) 2667–2688.

[15] K.W. Witwer, E.I. Buzás, L.T. Bemis, A. Bora, C. Lässer, J. Lötvall, M.G. Piper, S. Sivaraman, J. Skog, C. Théry, Standardization of sample collection, isolation and analysis methods in extracellular vesicle research, J. Extracell. Vesicles 2 (2013).

[16] A.N. Böing, E. van der Pol, A.E. Grootemaat, F.A. Coumans, A. Sturk, R. Nieuwland, Single-step isolation of extracellular vesicles by size-exclusion chromatography, J. Extracell. Vesicles 3 (2014).

[17] L. Pascucci, V. Coccè, A. Bonomi, D. Ami, P. Ceccarelli, E. Ciusani, L. Viganò, A. Locatelli, F. Sisto, S.M. Doglia, Paclitaxel is incorporated by mesenchymal stromal cells and released in exosomes that inhibit in vitro tumor growth: a new approach for drug delivery, J. Control. Release 192 (2014) 262–270.

[18] T. Yang, P. Martin, B. Fogarty, A. Brown, K. Schurman, R. Phipps, V.P. Yin, P. Lockman, S. Bai, Exosome delivered anticancer drugs across the blood–brain barrier for brain cancer therapy in *Danio rerio*, Pharm. Res. 1-12 (2015).

[19] Y. Toda, K. Takata, Y. Nakagawa, H. Kawakami, S. Fujioka, K. Kobayashi, Y. Hattori, Y. Kitamura, K. Akaji, E. Ashihara, Effective internalization of U251-MG-secreted exosomes into cancer cells and characterization of their lipid components, Biochem. Biophys. Res. Commun. 456 (2015) 768–773.

[20] L.A. Mulcahy, R.C. Pink, D.R.F. Carter, Routes and mechanisms of extracellular vesicle uptake, J. Extracell. Vesicles 3 (2014).

[21] M.S. Surapaneni, S.K. Das, N.G. Das, Designing paclitaxel drug delivery systems aimed at improved patient outcomes: current status and challenges, ISRN Pharmacol. 2012 (2012).

[22] G. Fuhrmann, A. Serio, M. Mazo, R. Nair, M.M. Stevens, Active loading into extracellular vesicles significantly improves the cellular uptake and photodynamic effect of porphyrins, J. Control. Release (2014).

[23] S.C. Jang, O.Y. Kim, C.M. Yoon, D. Choi, T. Roh, J. Park, J. Nilsson, J. Lötvall, Y. Kim, Y.S. Gho, Bioinspired exosome-mimetic nanovesicles for targeted delivery of chemotherapeutics to malignant tumors, ACS Nano 7 (2013) 7698–7710.

[24] T. Smyth, M. Kullberg, N. Malik, P. Smith-Jones, M.W. Graner, T.J. Anchordoquy, Biodistribution and delivery efficiency of unmodified tumor-derived exosomes, J. Control. Release 199 (2015) 145–155.

[25] D. Sun, X. Zhuang, X. Xiang, Y. Liu, S. Zhang, C. Liu, S. Barnes, W. Grizzle, D. Miller, H. Zhang, A novel nanoparticle drug delivery system: the anti-inflammatory activity of curcumin is enhanced when encapsulated in exosomes, Mol. Ther. 18 (2010) 1606–1614.

[26] K.J. Svensson, H.C. Christianson, A. Wittrup, E. Bourseau-Guilmain, E. Lindqvist, L.M. Svensson, M. Morgelin, M. Belting, Exosome uptake depends on ERK1/2-heat shock protein 27 signaling and lipid raft-mediated endocytosis negatively regulated by caveolin-1, J. Biol. Chem. 288 (2013) 17713–17724.

[27] C. Ferlini, L. Cicchillitti, G. Raspaglio, S. Bartollino, S. Cimitan, C. Bertucci, S. Mozzetti, D. Gallo, M. Persico, C. Fattorusso, Paclitaxel directly binds to Bcl-2 and functionally mimics activity of Nur77, Cancer Res. 69 (2009) 6906–6914.

[28] N. Kosaka, H. Iguchi, Y. Yoshioka, K. Hagiwara, F. Takeshita, T. Ochiya, Competitive interactions of cancer cells and normal cells via secretory microRNAs, J. Biol. Chem. 287 (2012) 1397–1405.

[29] O.P. Wiklander, J.Z. Nordin, A. O'Loughlin, Y. Gustafsson, G. Corso, I. Mager, P. Vader, Y. Lee, H. Sork, Y. Seow, N. Heldring, L. Alvarez-Erviti, C.E. Smith, K. Le Blanc, P. Macchiarini, P. Jungebluth, M.J. Wood, S.E. Andaloussi, Extracellular vesicle in vivo biodistribution is determined by cell source, route of administration and targeting, J. Extracell. Vesicles 4 (2015) 26316.

[30] T. Imai, Y. Takahashi, M. Nishikawa, K. Kato, M. Morishita, T. Yamashita, A. Matsumoto, C. Charoenviriyakul, Y. Takakura, Macrophage-dependent clearance of systemically administered B16BL6-derived exosomes from the blood circulation in mice, J. Extracell. Vesicles 4 (2015) 26238.